PROTEINS
STRUCTURE ■ FUNCTION ■ BIOINFORMATICS

A computational investigation on the role of glycosylation in the binding of alpha1 nicotinic acetylcholine receptor with two alpha-neurotoxins

Nikolaos Dimitropoulos, Athanasios Papakyriakou, Georgios A. Dalkas, Christos T. Chasapis, Konstantinos Poulas, and Georgios A. Spyroulias*

Department of Pharmacy, University of Patras, GR-26504, Patras, Greece

ABSTRACT

Based on the crystal structure of the extracellular domain (ECD) of the mouse nicotinic acetylcholine receptor (nAChR) alpha1 subunit bound to α-bungarotoxin (α-Btx) we have generated *in silico* models of the human nAChR α1 bound to α-Btx and α-cobratoxin (α-Cbtx), both in the presence and in the absence of the N-linked carbohydrate chain. To gain further insight into the structural role of glycosylation molecular dynamics (MD) simulations were carried out in explicit solvent so as to compare the conformational dynamics of the binding interface between nAChR α1 and the two toxins. An interesting observation during the course of the MD simulations is the strengthening of the receptor-toxin interaction in the presence of the carbohydrate chain, mediated through a shift in the position of the sugars towards the bound toxin. Critical protein–sugar interactions implicate residues Ser187 and Trp184 of nAChR and Thr6, Ser9, and Thr15 of α-Btx, as well as Thr6 and Pro7 of α-Cbtx. Analysis of the predicted residue-specific intermolecular interactions is intended to inspire biophysical studies on the functional role of glycosylation in the gating mechanism.

Proteins 2011; 79:142–152.
© 2010 Wiley-Liss, Inc.

Key words: nicotinic acetylcholine receptor; ligand-gated ion channels; glycosylation; α-neurotoxins; homology modeling; molecular dynamics simulations.

INTRODUCTION

Nicotinic acetylcholine receptors (nAChRs) are transmembrane glycoproteins which belong to the superfamily of the Cys-loop ligand-gated ion channels (LGICs), which also includes the GABA, glycine, and 5-HT3 receptors.[1–3] LGICs form homo- or hetero-pentamers of related subunits, and each of them consists of a large extracellular ligand-binding domain, a transmembrane region, and an intracellular region.[2] The most characteristic feature of this superfamily is a conserved sequence of 13 residues flanked by linked cysteines in the N-terminal domain of each subunit.[3] The extracellular domains (ECDs), which are ~210 residues long, contain binding sites for agonists and competitive antagonists. Binding of an agonist induces rapid opening of the transmembrane ion channel, leading to a change in membrane potential.[4,5]

nAChRs are divided in two groups: the muscle type and the neuronal type.[2] The muscle type is found in vertebrate skeletal muscle and in fish electric organs, while the neuronal type is found in the central and peripheral nervous system, and also in nonneuronal tissues. The muscle nAChR consists of five homologous subunits forming a channel with stoichiometry $(\alpha1)_2\beta\gamma\delta$ in embryos or $(\alpha1)_2\beta\varepsilon\delta$ in adults. Apart from its important physiological role, muscle type nAChR is the target in several inherited and acquired diseases.[6–8] The α1 subunit of nAChR has been broadly studied due to its unique characteristics. The ECD of the α1 chain contains both the binding sites for cholinergic ligands[2,9] and the major immunogenic region (MIR), the part of the subunit which is targeted by autoantibodies in the autoimmune disease myasthenia gravis.[10,11]

The presence of a certain subunit can affect the localization, biophysical, functional, and pharmacological properties of nAChRs and the regulation of the expression of the nAChR subtype at the developmental or adult stage, whereas the lack of a subunit may lead to the compensatory upregulation of other subtypes.[12] In the last years, the knowledge regarding the nAChR structure has been dramatically increased by the determination of (a) the electron microscopy structure of the Torpedo nAChR,[13] (b) the X-ray crystal structures of the ligand-free or ligand-bound molluscan ACh-binding

Additional Supporting Information may be found in the online version of this article.
Grant sponsor: EU FP7 "Neurocypres" project; Grant number: 202088.
*Correspondence to: G. A. Spyroulias, Department of Pharmacy, University of Patras, Panepistimioupoli, Rion, GR-26504, Greece. E-mail: G.A.Spyroulias@upatras.gr
Received 23 April 2010; Revised 6 August 2010; Accepted 19 August 2010
Published online 16 September 2010 in Wiley Online Library (wileyonlinelibrary.com).
DOI: 10.1002/prot.22867

© 2010 WILEY-LISS, INC.

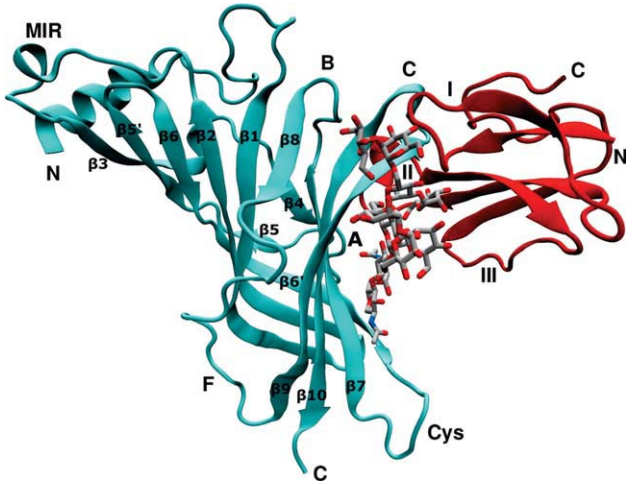

Figure 1

Crystal structure of the mouse nAChR α1-ECD bound to α-bungarotoxin (α-Btx). The receptor and the toxin are represented with cyan and red ribbons, respectively, while the carbohydrate chain is shown as a stick model with carbon atoms in silver, oxygen in red, and nitrogen in blue. [Color figure can be viewed in the online issue, which is available at wileyonlinelibrary.com.]

proteins (AChBPs),[14–21] (c) the X-ray crystal structure of the mouse nAChR α1-ECD bound to α-bungarotoxin (α-Btx),[22] and (d) the X-ray crystal structures of two prokaryotic LGICs; one from the bacterium *Erwinia chrysanthemi* (ELIC)[23] and another one from the bacterium *Gleobacter violaceus* (GLIC).[24,25]

The crystal structure of the mouse nAChR α1-ECD (α211) bound to α-Btx at 1.94 Å resolution revealed atomic details for several key functional elements of nAChR, such as the MIR, the signature Cys-loop and the carbohydrate chain linked to Asn141.[22] The structure of α211 (see Fig. 1) is organized around a hydrophobic core of 10 β-strands, joined through the Cys-loop, and contains one N-terminal α-helix. The sheet made of strands β1, β2, β3, β5, β6, and β8 is called the inner β-sheet, whereas the sheet made of strands β4, β7, β9, and β10 is called the outer β-sheet. The structure also contains several loops that are important for nAChR function. Loops β4-β5 (A), β7-β8 (B), and β9-β10 (C) form the ligand-binding site of the nAChR α1 subunit,[13,14,26] whereas Loops β1-β2, β6-β7 (Cys-loop), and β8-β9 (F) interact with the transmembrane domain and are involved in coupling of ligand-binding to channel opening.[27] The bound α-Btx on the outer sheet of the β-barrel (see Fig. 1) is a long-chain 74-a.a α-neurotoxin isolated from the *Bungarus multicinctus* venom. Its spatial structure comprises a central β-sheet from which protrude three finger-like loops (I–III) confined by four disulfide bonds, while a fifth SS-bond is found at the tip of the central loop (II).[28]

The ECDs of nAChR subunits contain various glycosylation sites. A highly conserved glycosylation site (found in all muscle and neuronal type subunits except α7, α8, and α9) is located in the Cys-loop residue Asn141.[6] This is the only glycosylation site of the α1 subunit. Several other conserved glycosylation sites are found in the other nAChR subunits. Most of the oligosaccharide chains in nAChR subunits are of the high-mannose type.[29] Several studies show that glycosylation is important for the surface expression and correct assembly of the receptor.[30,31] In the crystal structure of the mouse nAChR α1-ECD,[22] the Asn141-linked oligosaccharide chain stretches from the Cys-loop to the ligand-binding loops, and extensively interacts with the bound toxin. Functional studies,[22,32] suggest that the carbohydrate chain may be implicated in coupling ligand binding to channel gating. A more profound understanding of the general role of glycosylation in channel function requires further studies.

Several studies on nAChR that employ computational methods have been published in recent years.[33–38] In these studies, homology modeling and molecular dynamics (MD) are used as a means to explore ligand–receptor interactions at the atomic level, as well as to understand the molecular mechanisms involved in channel activation and inhibition. Templates used in the modeling of nAChRs are either the structure of the Torpedo nAChR,[13] or the various high-resolution X-ray structures of AChBPs.[14–21] Although these studies have provided great insight into the receptor–toxin interactions, the effect of the oligosaccharide moiety on toxin binding and receptor dynamics has not yet been explored.

In the present study homology modeling and MD simulations were employed with the aim to gain structural information on the role of glycosylation of the human nAChR α1-ECD in the binding with two neurotoxins, α-bungarotoxin (α-Btx), and α-cobratoxin (α-Cbtx). A detailed comparison between the glycosylated and the non-glycosylated models of both the mouse and the human nAChR α1 complexes with the two toxins revealed key intermolecular interactions at an atomic level. The explicit solvent representation allowed us to monitor water-mediated interactions, as well as the presence of ordered solvent molecules inside a hydrophobic pocket of α1, which have been proposed to have a functional role in the gating mechanism.[22]

COMPUTATIONAL METHODS

Homology modeling

Protein sequences of the mouse and the human nAChR α1 ECD were acquired from the SWISS/PROT database.[39] It should be noted that the term "mouse α1" is used to refer to the ECD construct that was used for crystallization with mutations at Val8Glu, Trp149Arg, and Val155Ala.[22] Sequence alignment was performed using ClustalW2,[40] which revealed a 95% identity as shown in Figure S1 (Supporting Information). The crys-

tal structure of the ECD of the mouse nAChR α1 subunit (PDB ID: 2QC1)[22] was used as a template for the human nAChR α1 ECD homology model. Twenty models were generated using MODELLER v7.2,[41] and the model with the lowest target function was selected as the initial structure of human nAChR α1 ECD. Validation of the model was performed using the Structural Analysis and Verification Server[42] and selected results are presented in the Supporting Information (Fig. S2).

Preparation of the models

The human nAChR α1 homology model and the template structure of the mouse α211-α-Btx complex (PDB ID: 2QC1) were superimposed with a backbone RMSD of 0.37 Å (a.a. 1-210). Subsequently, the crystallographic coordinates of α-Btx and of the carbohydrate chain from 2QC1 were used for the two models of the human nAChR, one with bound α-Btx in the presence of the N-linked sugars, and the other with bound α-Btx lacking the oligosaccharide moiety. The coordinates of α-Cbtx were retrieved from the X-ray structure of the AChBP bound toxin (chain F from PDB ID 1YI5)[16] and was superimposed on the α-Btx molecule within the mouse α211 complex using the MultiSeq module of VMD 1.8.6[43] as shown in Figure S3 (Supporting Information). Following the same procedure as described above, two models of the human nAChR-α-Cbtx complex were prepared (with and without the carbohydrate chain). For reference purposes, a model of the mouse α211-α-Btx complex lacking the oligosaccharide was prepared by removing the sugar atoms from 2QC1.

All crystallographic water molecules were discarded from the initial models. Missing heavy and hydrogen atoms were added using the XLEaP module of AMBER 9.[44] All basic residues were protonated and all acidic residues were deprotonated. Histidine protonation states were manually set by examining their potential for hydrogen bonding with surrounding residues, and by taking into account the pKa values calculated using the H++ web server.[45] Specifically, His79, His115, and His134 of α1 ECD, His4 of α-Btx and His18 of α-Cbtx were set to be protonated at $N^{\delta 1}$, while His3, His25, His186, and His204 of α1 ECD, and His68 of α-Btx were set to be protonated at $N^{\varepsilon 2}$. The improved protein backbone AMBER force field, denoted as ff99SB, was employed for all protein atoms,[46,47] while the carbohydrate chain was represented using the GLYCAM06 force field.[48] To relax the models from crystal-packing contacts and optimize the position of the new atoms a set of minimization steps was carried out using the SANDER module of AMBER 9.[44] In particular, 1000 steps were performed in order to allow relaxation of the hydrogen atoms only, using the steepest descent algorithm. Then, 1000 steps of conjugate gradient minimization were carried out by restraining all Cα atoms using positional harmonic restraints of 50 kcal mol^{-1} $Å^{-2}$ force constant. A third round of unrestrained minimization was carried out for 3000 steps. The generalized Born implicit solvation model (GB^{HCT})[49] was employed throughout the energy minimizations with a 16-Å cutoff for the nonbonded interactions.

Molecular dynamics and analysis

AMBER 9 was used for all the MD calculations carried out on Intel Xeon workstations. Numerical integration was performed with a 2-fs time step and all bonds involving hydrogen atoms were constrained with SHAKE.[50] Periodic boundary conditions were imposed using the particle mesh Ewald method[51] with 8 Å limit for the direct space sum. Temperature and pressure controls were imposed using a Berendsen-type algorithm,[52] both with 1 ps coupling constants. All receptor-toxin models were immersed in isometric truncated octahedron TIP3P-water boxes,[53] and the appropriate number of counter ions was added to neutralize the total charge. The following procedure was used so as to optimize the position of the solvent molecules and equilibrate the temperature and pressure of the systems: (a) energy minimization for 1000 steps using the steepest descent method with harmonic restraints of 50 kcal mol^{-1} $Å^{-2}$ force constant on all solute atoms; (b) restrained constant volume dynamics (NVT ensemble) at 300 K for 30 ps; (c) a second energy minimization for 1000 steps with 10 kcal mol^{-1} $Å^{-2}$ restraints on all protein Cα atoms; (d) temperature was then gradually increased to 300 K within six rounds of 5-ps constant volume dynamics (NVT), while solute atoms were restrained with 10 kcal mol^{-1} $Å^{-2}$; (e) restraints were then gradually released within 20 ps in the NVT ensemble at 300 K; (f) the density of the systems was increased to 1.0 g cm^{-3} during 150 ps of constant pressure dynamics (NPT ensemble). Subsequently, production runs were carried out under physiological conditions (300 K, 1 atm) in the NPT ensemble for a total time of 20 ns (overviewed in Table SI in Supporting Information). The translational centre-of-mass motion was removed every 1000 steps and trajectories were updated every 500 steps. To assess the validity of our observations all runs were repeated with different initial velocity assignment starting from equilibration Step d (vide supra). In particular, for the simulation of the crystal structure of mouse α211-α-Btx complex validation was performed by a second 20-ns MD run in which all the crystallographic water molecules (PDB ID: 2QC1) were preserved.

Processing of the MD trajectories was performed using the PTRAJ module of AMBER 9, while VMD 1.8.6[43] was used for their examination. MD trajectories were analyzed to identify important intermolecular interactions by extracting their geometric features (distances and angles) as a function of simulation time. Hydrogen bonding

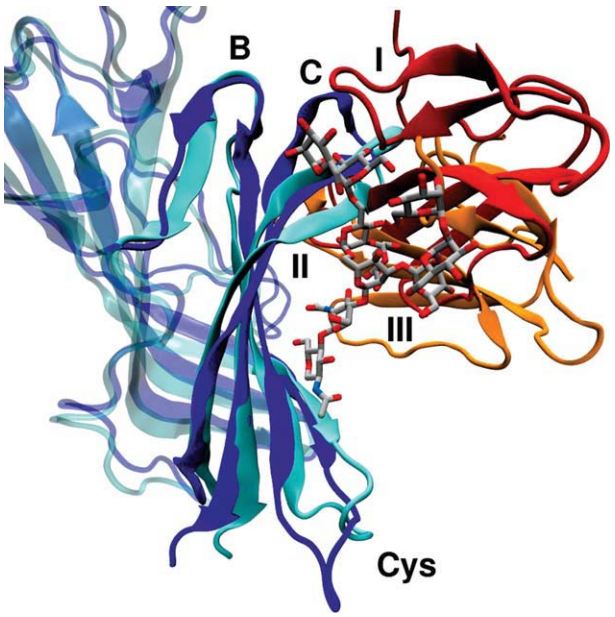

Figure 2

Comparison of the non-glycosylated and the glycosylated model of the mouse α1 ECD-α-Btx complex after 20 ns of MD simulations. The α1 ECD is shown in blue and cyan for the non-glycosylated and the glycosylated model, respectively, while the corresponding α-Btx molecules are shown in red and orange. The carbohydrate chain is shown with carbon atoms in silver sticks, oxygen atoms in red, and nitrogen atoms in blue.

interactions were monitored using a 3.4 Å distance cutoff and 120° as the angle cutoff. Hydrophobic interactions were included for a pair of carbon atoms separated by a distance less than 4.0 Å. Only interactions present for more than half of the simulation time were considered. Water-mediated hydrogen bonds were considered if observed in at least 25% of the trajectory frames. Figures were prepared using VMD and plots using Grace.

RESULTS AND DISCUSSION

Mouse α1 ECD-α-Btx complex

With the aim to examine the effect of the oligosaccharide moiety on the mouse α1 ECD bound to α-Btx, two independent 20-ns MD simulations were performed for the non-glycosylated and the glycosylated models of the complex. The models were based on the single α1 subunit out of the pentameric receptor, which represents the principal component of the binding side.[2] The use of the α1 mouse nAChR crystal structure (PDB ID: 2QC1) as a template was preferred because of its high resolution (1.94 Å) and its high homology with the human α1 subunit (Fig. S1 in Supporting Information). On the other hand, a pentameric model of human nAChR would be based either on the low-resolution Torpedo AChR electron microscopy studies[13] or on the various high-resolution crystal structures of AChBPs, which exhibit low homology for human nAChR.[14–21] Superposition of the human nAChR α1 homology model with the pentameric Torpedo AChR structure showed that the carbohydrate chain does not interact with the neighboring non-alpha subunits, and no major clashes occur between the toxin and the complementary component of the binding site. Therefore, the results generated by the MD simulations are not significantly affected by the absence of the neighboring subunits. The transmembrane domain of the α1 subunit was also not modeled, since the structure of Torpedo nAChR[13] has shown that the transmembrane domain interacts with the β1-β2 loop and the Cys loop of the extracellular domain, and does not actively take part in toxin binding.

In the non-glycosylated model (see Fig. 2), the α-Btx central loop (Finger II) is positioned deep inside the binding pocket, between Loops A, B, and C of mouse α1, while the α-Btx Finger I and C-terminal loop are also in close proximity with Loop C. Finger III of α-Btx does not interact with the α1 ECD. The binding of α-Btx to α1 is stabilized by extensive interactions between individual residues (Table I). In particular, the Finger II Arg36 is hydrogen bonded to Arg149 in Loop B and Tyr190 and Cys192 in Loop C, and participates in π-cation interactions with Phe32 of α-Btx and Tyr190 and Tyr198 (both in Loop C) for the entire course of the MDs. The guanidinium moiety of Arg36 closely resembles the position of the quaternary ammonium group of a bound agonist molecule in AChBP crystal structures.[15,19] The introduction of a positively-charged residue in the ligand-binding pocket is critical for the competitive antagonism of neurotoxins.[54] Several other

Table I

Residue Specific Interactions of α-Btx with the Non-glycosylated and the Glycosylated ECD of Mouse nAChR α1 Subunit

α-Btx	Mouse α1 ECD	Mouse α1 ECD with carbohydrate chain
Finger I		
Thr6		Phe189
Pro10	Thr195	Thr195
Ile11	Phe189, Pro194	Phe189, **Pro194**
Finger II		
Asp30		**Tyr190**
Val31	Tyr93	Tyr93
Phe32	Val91, Tyr93, Tyr190	Tyr93, Tyr190
Arg36	**Arg149, Tyr190, Cys192**, *Tyr198*	**Tyr190**, **Cys192**, *Tyr198*
Lys38	**Ser191**	**Ser191**
Val39	Val188, Tyr190	Val188, Tyr190
Val40	**Phe189**	**Phe189**
C-ter loop		
His68	**Tyr190**, Pro194	**Tyr190**, Pro194
Pro69	Pro194	
Lys70		Pro194

Residues involved in van der Waals interactions are in plain font, those forming hydrogen bonds are in bold, and those involved in π-cation interactions in italic.

Table II
Protein–Sugar Interactions Observed in the Simulation of the Mouse nAChR α1 ECD Bound to α-Btx

Carbohydrate	Mouse α1 ECD	α-Btx
NAG2	His204	
NAG3	(**Trp184**), **His186**, His204	
MAN4	Trp184	
MAN5	His186, **Trp187**	**Thr6**
MAN6	Trp187, Pro197	**Ser9**
MAN8	His186, Phe189	**Thr6**, (**Val40**), (**Glu41**)

Residues involved in van der Waals interactions are in plain font, those forming hydrogen bonds are in bold and those forming water-mediated hydrogen bonds are in brackets.

contacts are observed between Finger II and Loop C (Table I). These interactions are also observed in the crystal structure of the mouse α1 bound to α-Btx.[22]

The N-glycosylated mouse α1-α-Btx model exhibits analogous interactions with the non-glycosylated model (Table I). Finger II of α-Btx inserts into the binding site, while Finger II and the C-terminal loop are wrapped around Loop C of the α1 ECD. Arg36 is involved in π-cation interactions with Phe32 of α-Btx and Tyr190, Tyr198 of Loop C and also forms hydrogen bonds with Tyr190 and Cys192. Additionally, Asp30 in Finger II forms a hydrogen bond with the side chain OH of Tyr190. The carbohydrate chain linked to Asn141 interacts both with the α1 ECD and the toxin molecule, consistent with the crystal structure,[22] providing a network

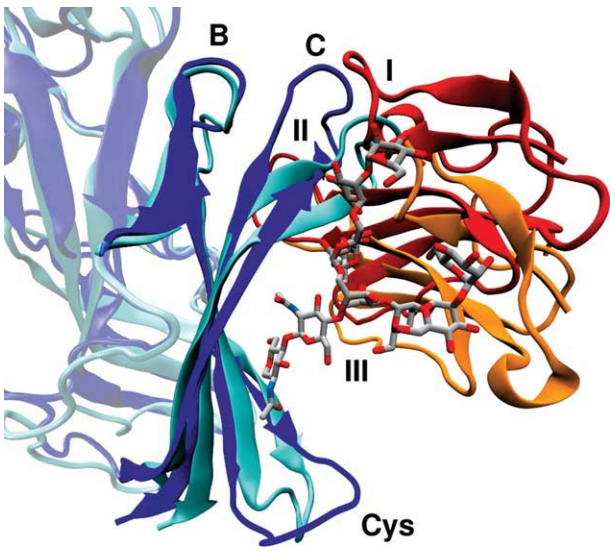

Figure 3
Superposition of the non-glycosylated and the glycosylated model of the human α1 ECD-α-Btx complex, after 20 ns of MD simulations. The α1 ECD is shown in blue and cyan for the non-glycosylated and the glycosylated model, respectively, while the corresponding α-Btx molecules are shown in red and orange. The carbohydrate chain is shown with carbon atoms in silver sticks, oxygen atoms in red, and nitrogen atoms in blue. [Color figure can be viewed in the online issue, which is available at wileyonlinelibrary.com.]

Table III
Comparison of the Toxin–Receptor Interactions Between the Non-glycosylated and the Glycosylated Models of Human nAChR α1 ECD Bound to α-Btx

α-Btx	Human α1 ECD	Human α1 ECD with carbohydrate chain
Finger I		
Th6		Thr189, (**Pro194**)
Thr8		(**Pro194**)
Ile11	Thr189, **Pro194,**	Pro194
Finger II		
Asp30		(**Tyr190**)
Val31	Tyr93, Trp149	Tyr93, Trp149
Phe32	Tyr93, Trp149, Tyr190	Tyr93, Trp149, Tyr190
Arg36	*Tyr93*, **Thr148**, *Trp149*, **Tyr190**, **Cys192**, *Tyr198*, (**Leu199**)	*Tyr93*, *Trp149*, **Tyr190**, **Cys192**, *Tyr198*
Lys38	**Ser191**	**Ser191**
Val39	Val188, Tyr190	Val188, Tyr190
Val40	**Thr189**	**Thr189**
C-ter loop		
His68	**Tyr190**, Pro194	Pro194
Pro69		Pro194
Lys70	**Cys192**	

Residues involved in van der Waals interactions are in plain font, those forming hydrogen bonds are in bold, those forming water-mediated hydrogen bonds are in brackets and those involved in π-cation interactions in italic.

of sugar—nAChR/toxin interactions monitored during the entire MD course (Table II). In the backside of Loop C, Trp187 is found to be hydrogen bonded to MAN5 via its backbone, as well as making van der Waals contacts with MAN6. The mannoses MAN5, MAN6, and MAN8 interact with toxin Finger I through several hydrogen bonds with Thr6 and Ser9. Furthermore, MAN8 reaches out to the base of Finger II, forming water-mediated hydrogen bonds with Val40 and Glu41.

Human α1 ECD-α-Btx complex

MD simulations were carried out for the models of human α1 bound to α-Btx for 20 ns under the same conditions as for the models of mouse α1 (see Fig. 3). In the non-glycosylated model, the predicted α1-toxin interactions are very similar to the mouse α1-toxin model. Finger II contacts Loops A, B, and C, while Finger I and the C-terminal loop of α-Btx interact with Loop C. Finger III is distant from the nAChR subunit and does not interact with it. A significant difference from the mouse model is the substitution of Arg149 (mutated in α211 to increase solubility and achieve crystallization) with Trp149 in human nAChR α1. Trp149 is highly conserved amongst nAChR alpha subunits and AChBP, as it was shown to play a critical role in agonist and antagonist binding.[14,55] In our model Trp149 confirms its significant role as it is involved in π-cation and van der Waals interactions with the toxin residues Arg36, Val31, and Phe32. Several other Loop C residues are involved in the binding of α-Btx (Table III).

Table IV
Protein–Sugar Interactions Observed in the Simulation of Human α1 ECD Bound to α-Btx

Carbohydrate	Human α1 ECD	α-Btx
NAG2	His204	
NAG3	**Trp184, His186**	
MAN5	**Ser187**	
MAN6	**Ser187**	**Thr6, Ser9**
MAN7		**Ser9**
MAN8	**Ser187**, Val188, **Thr189**	**Thr6, Val40**
MAN11		Ala7, Val14, **Thr15**

Residues involved in van der Waals interactions are in plain font and those forming hydrogen bonds are in bold.

In the glycosylated model, the binding of α-Btx displays the usual structural features. Most residue-specific contacts are the same to the non-glycosylated model (Table III). A striking difference is the increased contacts between toxin Finger I and the nAChR subunit. These contacts are the result of a shift in the toxin position, which aligns the β-strand of Finger I with the sugars (see Fig. 3). Additionally, the toxin molecule interacts heavily with the sugar chain (Table IV). The mannoses mainly interact with residues 184-188 in strand β9 and in particular with Ser187, which engages in hydrogen bonds with mannoses MAN5, MAN6, and MAN8. At the same time

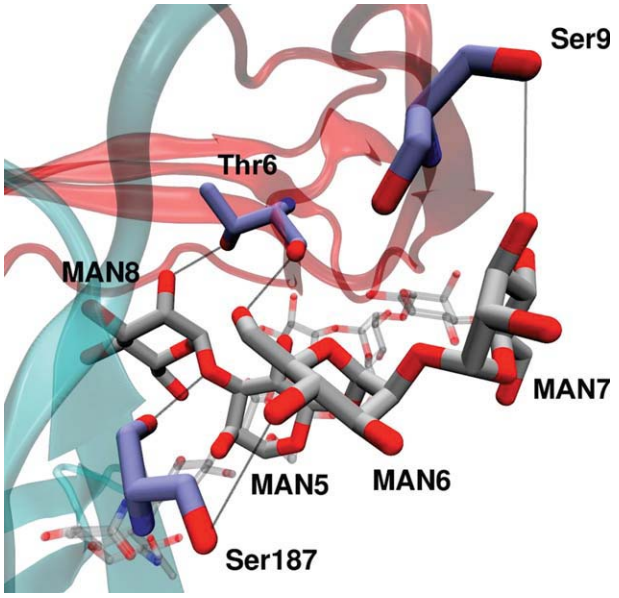

Figure 4
Close-up view of the human α1 ECD-α-Btx model (after 20 ns of simulation) showing the sugar moieties that mediate the interaction between Ser187 of α1 and Thr6 and Ser9 of α-Btx. The α1 ECD and α-Btx are shown in cyan and red ribbons, respectively. The carbohydrate chain is shown with carbon atoms in silver sticks, while the displayed α1 and toxin residues are shown with carbon atoms in light blue sticks. In both cases oxygen atoms are shown in red and nitrogen atoms are in dark blue. [Color figure can be viewed in the online issue, which is available at wileyonlinelibrary.com.]

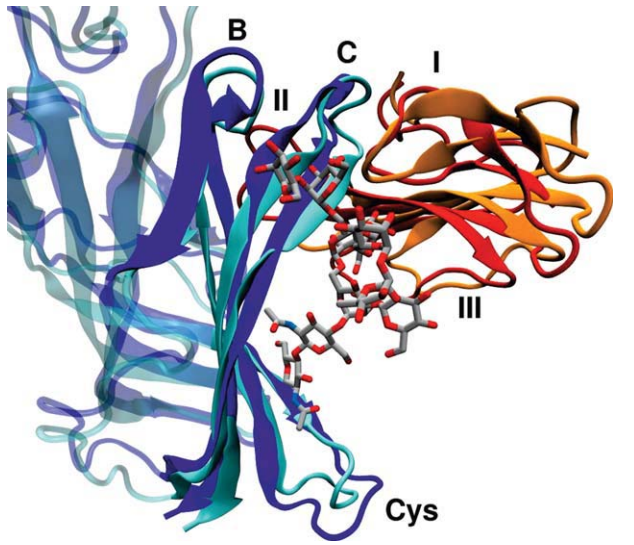

Figure 5
Comparison of the non-glycosylated and the glycosylated models of human α1 ECD-α-Cbtx complex, after 20 ns of MD simulations. The α1 ECD is shown in blue and cyan for the non-glycosylated and the glycosylated model, respectively, while the corresponding α-Cbtx molecules are shown in red and orange. The carbohydrate chain is shown with carbon atoms in silver sticks, oxygen atoms in red, and nitrogen atoms in blue. [Color figure can be viewed in the online issue, which is available at wileyonlinelibrary.com.]

MAN6 and MAN8 make contacts with toxin residues. Therefore the carbohydrate chain acts as a bridge between α1 and α-Btx (see Fig. 4). Additional interactions between the sugars and α-Btx are located both in the loop (Thr6, Ala7, Ser9) and the β-strand (Val14, Thr15) of the toxin's Finger I. In analogy to the models of mouse α1, MAN8 exhibited water-mediated contacts with Finger II, and especially with Val40 a direct hydrogen bond can be observed.

Human α1 ECD-α-Cbtx complex

Alpha-cobratoxin (α-Cbtx) is a long-chain α-neurotoxin (71 amino acid residues) from the venom of *Naja siamensis*. Like α-Btx, its spatial structure is the characteristic "three-finger fold."[56] Models of α-Cbtx bound to the human α1 ECD were built and subjected to 20 ns of MDs (see Fig. 5). In the non-glycosylated model, the binding of α-Cbtx is largely similar to that of α-Btx. Loop C of α1 is tightly surrounded by Fingers I–II and C-terminal loop of α-Cbtx. Finger II inserts into the binding site of α1, with Arg33 (corresponding to Arg36 in α-Btx) and Phe29 (Phe32 in α-Btx) forming a strong π-cation interaction system with Tyr93, Trp149, Tyr190, and Tyr198, as observed in the crystal structure of α-Cbtx bound to AChBP.[16] Arg33 additionally displays numerous hydrogen bonds with Thr148, Thr149 (water-mediated), Tyr190, Cys192, and Leu199 (water-

Table V
Comparison of the Toxin–Receptor Interactions Between the Non-glycosylated and the Glycosylated Models of Human nAChR α1 ECD Bound to α-Cbtx

α-Cbtx	Human α1 ECD	Human α1 ECD with carbohydrate chain
Finger I		
Pro7	(**Pro194**), Pro197, Thr189	Pro197
Ile9	Pro194	Pro197
Finger II		
Asp27	(**Tyr190**)	
Ala28	Val91, (**Tyr93**), (**Asp99**), Phe100, Trp149	
Phe29	Val91, Tyr93, Trp149, Tyr190	Tyr93, Trp149, Tyr190
Ile32	Trp149	Trp149
Arg33	**Thr148**, (**Trp149**), **Tyr190, Cys192**, *Tyr198*, (**Leu199**)	*Tyr93*, *Trp149*, *Tyr190*, **Cys192**, *Tyr198*
Lys35	**Ser191**	**Ser191**
Arg36	**Tyr93**, *Tyr198*, Asp200	
Val37	**Thr189**	**Thr189**
C-ter loop		
Phe65	Pro194	Pro194
Thr67		**Ser191**

Residues involved in van der Waals interactions are in plain font, those forming hydrogen bonds are in bold, those forming water-mediated hydrogen bonds are in brackets, those forming salt bridges are underlined and those involved in π-cation interactions in italic.

mediated). The nearby Arg36 is placed at the bottom of Loop C, forming a hydrogen bond with Tyr93 and a salt bridge with Asp200. Several other residues of α-Cbtx are involved in hydrogen bonds and van der Waals interactions with α1 residues (Table V).

The glycosylated model displays a small variation in the position of the bound toxin compared to the non-glycosylated model (see Fig. 5). During the simulation, the toxin molecule moves away from Loop A and places over the sugar chain (Table IV). At the same time, the carbohydrate chain moves away from its initial position and shifts closer to the toxin Finger I in a similar way as the human α1–α-Btx model. As a result, the toxin-loop C and toxin–sugar interactions are enhanced, while several contacts with Loops A and B are lost (Table V). The

Table VI
Protein–Sugar Interactions Observed in the Simulation of Human α1 ECD Bound to α-Cbtx

Carbohydrate	Human α1 ECD	α-Cbtx
NAG2	Ile131, His204, Val206	
NAG3	Trp184, (**Lys185**), **His204**	
MAN4	Trp184	
MAN5	Trp184, His186, **Ser187**	Pro7
MAN6	Trp184	Pro7
MAN7	Trp184, **Lys185**	
MAN8	**His186**, Val188, (**Thr189**)	**Thr6**, Pro7, (**Val37**), **Asp38**
MAN11		Ile5, **Thr6**, Pro7

Residues involved in van der Waals interactions are in plain font, those forming hydrogen bonds are in bold and those forming water-mediated hydrogen bonds are in brackets.

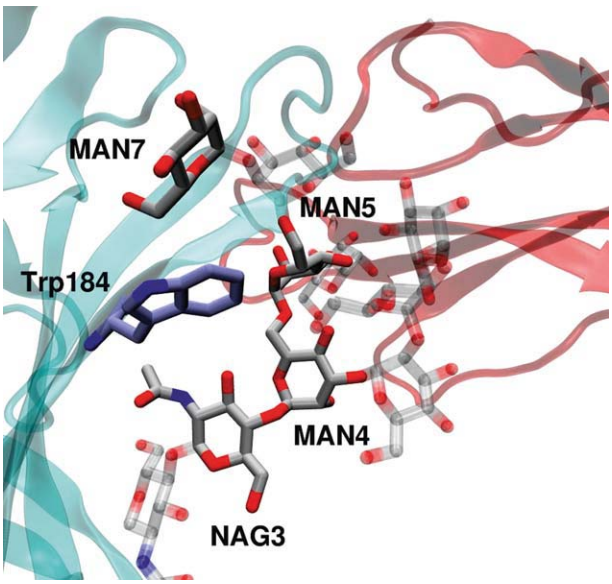

Figure 6
Close-up view of the protein–sugar interactions within the human α1 ECD-α-Cbtx complex. The α1 ECD and α-Cbtx are shown in cyan and red ribbons, respectively. The carbohydrate chain is shown with carbon atoms in silver sticks, while residue Trp184 from α1 is shown with carbon atoms in light blue sticks. In both cases oxygen atoms are shown in red and nitrogen atoms are in dark blue. [Color figure can be viewed in the online issue, which is available at wileyonlinelibrary.com.]

α1 ECD–sugar interactions are summarized in Table VI. The carbohydrate chain seems wrapped around Trp184, which makes van der Waals interactions with NAG3, MAN4, MAN5, MAN6, and MAN7, and therefore stabilizes their conformation (see Fig. 6). Additionally, MAN5 forms two hydrogen bonds with the NH and CO groups of Ser187. Finger I of α-Cbtx makes several interactions with the sugars. MAN8 forms hydrogen bonds with residues Thr6, Val37, and Asp38. The mannoses MAN5, MAN6, and MAN8 exhibit van der Waals contacts with Pro7. MAN11 also comes close enough to form contacts with the toxin, albeit short-lived in comparison to the other mannoses. The sugars MAN5 and MAN8 are critical anchor points for the conformation of the carbohydrate chain, as they are involved in numerous interactions with both the α1 ECD and the toxin molecule.

Comparison of the mouse model with the crystal structure

The crystal structure of the mouse α1-ECD bound to α-Btx provides a high-resolution view of nAChR α1 with the N-linked oligosaccharide chain and the bound toxin. Modeling of the non-glycosylated mouse α1 subunit revealed minor differences in comparison with the glycosylated structure, which mainly comprise small variations in the conformation of the loops. On the contrary, the binding mode of α-Btx is dependent on the presence of

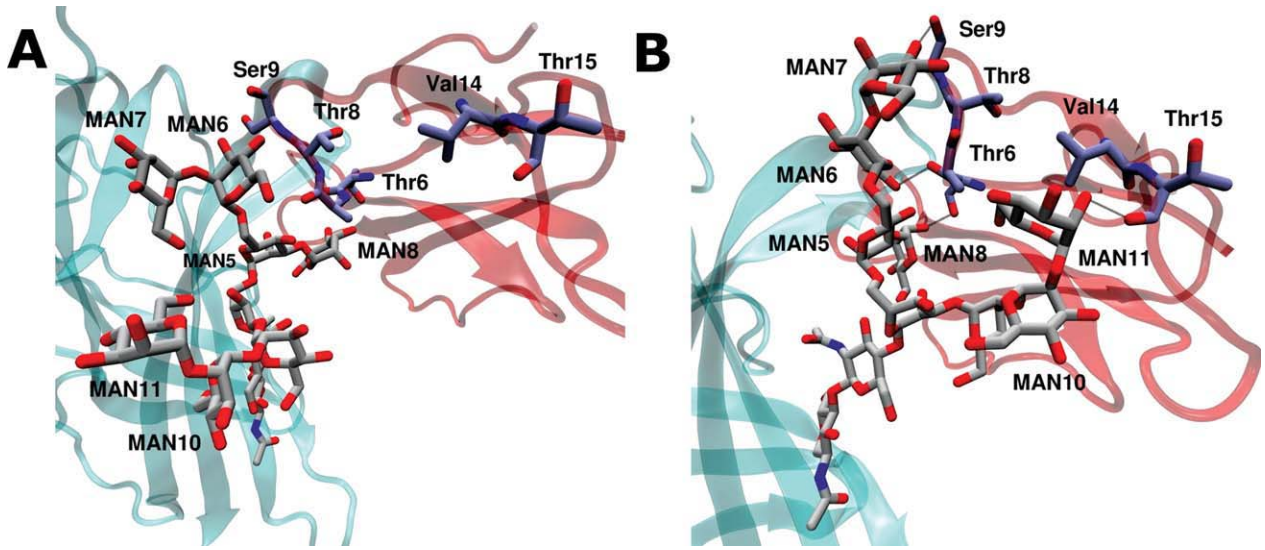

Figure 7

Snapshots of the human nAChR α1 ECD in complex with α-Btx taken at the beginning (**A**) and at the end (**B**) of the MD simulations. The α1 ECD and α-Btx are shown in cyan and red ribbons, respectively. The carbohydrate chain is shown with carbon atoms in silver sticks, while the toxin residues are shown with carbon atoms in light blue sticks. In both cases oxygen atoms are shown in red and nitrogen atoms are in dark blue. [Color figure can be viewed in the online issue, which is available at wileyonlinelibrary.com.]

the sugars. After 20 ns of MDs, the nonsugar model displays a disparity in the position of the bound toxin compared to the crystal structure. While the toxin Finger II is correctly placed inside the binding pocket, surrounded by Loops A, B, and C of the α1 ECD, the rest of the molecule is bent upward. This distorted position is the result of a movement of the toxin molecule during the course of the simulation. After the second nanosecond of simulation the toxin swings upward, so that Finger I and the C-terminal move closer to the upper part of Loop C (α1). Conversely, in the glycosylated model α-Btx is much less mobile and remains relatively close to the sugars. Finger I is sandwiched between Loop C and the sugar chain. The mannoses interact with the toxin and stabilize its position. Therefore the change in the first model can be attributed to the lack of interaction with the Asn141-linked carbohydrate chain.

The crystal structure of the mouse α1 bound to α-Btx revealed a hydration pocket inside the β-sandwich core of nAChR. This site harbors a well-ordered water molecule bonded to two buried hydrophilic residues, Thr52 and Ser126. The hydration cavity is also connected to the surface residue Asn94 on Loop A through a second ordered water molecule. Experimental data suggest that this hydrophilic interior of nAChR is important for channel function.[22] Our MD study can confirm the ability of this site to accommodate solvent molecules, since all the initial models lacked the crystallographic waters (see Computational Methods). In this way we were able to observe the entrance of water molecules into the cavity during the course of the MD simulations. The most stable and long-lived water molecule mediated the interaction between Thr52 and Ser126 (designated as W1 in Fig. S4 of the Supporting Information). The second water molecule that entered the cavity mediated hydrogen bonding interactions between Asn94 and Ser126 (W2 in Fig. S4, Supporting Information). Both bridging interactions were observed in all the MD simulations, albeit at different time frames.

Differences between mouse and human models

Since the modeling of human nAChR α1 ECD bound to α-Btx was based on the mouse α1 crystal structure, the two complexes exhibit a strong similarity. The β-sandwich cores of both human and mouse α1 superimpose very well, while the loops show slightly different trajectories. The binding of α-Btx is similar despite its position is slightly changed in the human model. An important difference is found in the core of the binding site: the mouse mutant α211 (which was used for crystallization) has an arginine residue in position 149, while the human α1 has a tryptophan in its place. Various studies indicate Trp149 as a critical residue for agonist and antagonist binding.[14,55] In the human α1 models Trp149 is involved in π-cation interactions with Arg36 of α-Btx, contributing in the toxin binding. On the other hand, the Phe189Thr substitution in Loop C has a small impact in the predicted receptor–toxin interactions.

The N-linked sugar chain behaves differently in the two models of α1. In the mouse model it is slightly per-

turbed from the initial, crystallographic position for the majority of the simulation time. The terminal mannose MAN11 remains distant from the toxin molecule. Conversely in the human model the sugars display an outward movement after the first nanosecond of the simulation (see Fig. 7). Specifically, the oligosaccharide moiety moves away from the outer β-sheet of α1 and towards the bound toxin molecule, while the toxin Finger I shifts downward and closer to the sugars. This movement brings mannose MAN11 in close contact to α-Btx and makes possible the formation of two hydrogen bonds with the sidechain of Thr15 [Fig. 7(B)].

The human α1 residue Ser187 is involved in two hydrogen bonds with the mannose MAN5 and another one with MAN8, while also interacting with Thr8 and Ser9 of α-Btx (see Fig. 4). Residing in the backside of Loop C, Ser187 keeps the sugar chain close to the toxin molecule, favoring interactions with it. In mouse α1 Ser187 is substituted by Trp187, which forms only one hydrogen bond with MAN5. Therefore, we can hypothesize that the Trp187Ser substitution in human α1 stabilizes the sugar chain in a conformation close to α-Btx.

Role of glycosylation in toxin binding

The crystal structure of the mouse α1 ECD bound to α-Btx revealed extensive interactions between α1 and the toxin that are mediated by the carbohydrate chain.[22] These results provided the structural basis of the key role of glycosylation on the high-affinity binding of α-Btx with nAChR α1 ECD, as shown by previous studies.[32] In addition, deglycosylation experiments implicated the involvement of the carbohydrate chain in the gating mechanism of the channel.[22] In an effort to provide further structural data on the role of glycosylation in the binding of toxins with human α1, we calculated the dynamics of two toxins bound to human α1 in the presence and in the absence of the sugars. In both cases, the modeled α1 ECDs superimposed very well, with slight variations in the conformation of the various loops, namely Loops A, B, C, and the Cys-loop. The difference between the glycosylated and non-glycosylated models lies in the binding mode of the toxin (Figs. 3 and 5). Throughout the MD simulations the position of the bound toxin molecule is shifted closer to the sugar chain in both the sugar models. The adjacent Loop C of α1 also shifts toward the sugar chain, and the toxin Finger I is engulfed between Loop C and the carbohydrates. Additionally, the sugar chain also changes conformation during the MDs, and moves closer to Finger I (see Fig. 7). In the case of α-Btx, the toxin shifts downward, bringing its Finger I close to the mannoses and favoring interactions with them. A long-lived hydrogen bond between MAN11 and Thr15, located in the β-strand of Finger I, greatly exemplifies the closeness of the sugar chain to the toxin molecule. The difference in toxin position is also observed in the case of α-Cbtx (see Fig. 5). In this case, Finger II is not inserted as deeply inside the binding site as in the other models. Loop C partially adopts a more open conformation due to its interaction with Finger I of α-Cbtx. As a result, the toxin-loop C and toxin–sugar interactions are increased. Trp184 and Ser187 are important residues implicated in the anchoring of the carbohydrate chain to the α1 subunit. The mannoses MAN5 and MAN8 are sandwiched between the toxin and the nAChR ECD and mediate their binding. On the other branch of the sugar chain, MAN11 is attached to the backside of toxin Finger I. The above findings confirm the role of the sugars in the binding of the toxins. The MD simulations revealed dynamic features relevant to function that were not anticipated from the crystal structure. Interesting is the fact that the binding mode of the toxins is different when the nAChR subunit is glycosylated. These sugar-mediated interactions actively take part in toxin binding and therefore could be related to channel activation.

CONCLUSIONS

The present study provides further insights into the binding of neurotoxins to nicotinic acetylcholine receptors. Using the crystal structure of the mouse nAChR α1-ECD (α211) bound to α-Btx as template we calculated models of the human nAChR α1-ECD bound to two long chain α-neurotoxins, α-Btx and α-Cbtx. The role of the oligosaccharide chain linked to residue Asn141 in toxin binding was explored, and important interactions between the sugars and the bound toxins were identified. More specifically, in the human models the conformation of the sugar chain changes during the simulation period. The sugars attach to Finger I of the bound toxin, mainly to residues Thr6, Ser9, and Thr15 of α-Btx, and Thr6–Pro7 of α-Cbtx. Ser187 was found to be a crucial residue for the anchoring of the sugar chain in a close position to α-Btx, while Trp184 seems equally important in the case of α-Cbtx. In particular, mannoses MAN5 and MAN8 engage in numerous contacts that stabilize the interaction of the toxin with the α1 subunit. Interestingly, our MD simulations of the human α1 ECD-toxin complexes confirmed the possible accommodation of two water molecules into a hydration cavity, which has been observed in the crystal structure of the mouse α1 ECD. These water-mediated interactions stabilize the position of three buried, hydrophilic residues, Thr52, Asn94 and Ser126, which may contribute to the gating mechanism of the receptor. These findings provide additional structural data that are expected to guide further biological studies on the structure and function of nAChRs.

REFERENCES

1. Corringer PJ, Le Novere N, Changeux JP. Nicotinic receptors at the amino acid level. Annu Rev Pharmacol Toxicol 2000;40:431–458.
2. Kalamida D, Poulas K, Avramopoulou V, Fostieri E, Lagoumintzis G, Lazaridis K, Sideri A, Zouridakis M, Tzartos SJ. Muscle and neu-

ronal nicotinic acetylcholine receptors. Structure, function and pathogenicity. FEBS J 2007;274:3799–3845.
3. Lester HA, Dibas MI, Dahan DS, Leite JF, Dougherty DA. Cys-loop receptors: new twists and turns. Trends Neurosci 2004;27:329–336.
4. Arias HR. Localization of agonist and competitive antagonist binding sites on nicotinic acetylcholine receptors. Neurochem Int 2000;36:595–645.
5. Changeux JP, Edelstein SJ. Allosteric receptors after 30 years. Neuron 1998;21:959–980.
6. Lindstrom JM. Acetylcholine receptors and myasthenia. Muscle Nerve 2000;23:453–477.
7. Fostieri E, Kostelidou K, Poulas K, Tzartos SJ. Recent advances in the understanding and therapy of myasthenia gravis. Future Neurol 2006;1:799–817.
8. Barrantes FJ, Aztiria E, Rauschemberger MB, Vasconsuelo A. The neuronal nicotinic acetylcholine receptor in some hereditary epilepsies. Neurochem Res 2000;25:583–590.
9. Tzartos SJ, Barkas T, Cung MT, Mamalaki A, Marraud M, Orlewski P, Papanastasiou D, Sakarellos C, Sakarellos-Daitsiotis M, Tsantili P, Tsikaris V. Anatomy of the antigenic structure of a large membrane autoantigen, the muscle-type nicotinic acetylcholine receptor. Immunol Rev 1998;163:89–120.
10. Tzartos SJ, Kokla A, Walgrave SL, Conti-Tronconi BM. Localization of the main immunogenic region of human muscle acetylcholine receptor to residues 67-76 of the alpha subunit. Proc Natl Acad Sci USA 1988;85:2899–2903.
11. Tzartos SJ, Cung MT, Demange P, Loutrari H, Mamalaki A, Marraud M, Papadouli I, Sakarellos C, Tsikaris V. The main immunogenic region (MIR) of the nicotinic acetylcholine receptor and the anti-MIR antibodies. Mol Neurobiol 1991;5:1–29.
12. Gotti C, Clementi F. Neuronal nicotinic receptors: from structure to pathology. Prog Neurobiol 2004;74:363–396.
13. Unwin N. Refined structure of the nicotinic acetylcholine receptor at 4A resolution. J Mol Biol 2005;346:967–989.
14. Brejc K, van Dijk WJ, Klaassen RV, Schuurmans M, van Der Oost J, Smit AB, Sixma TK. Crystal structure of an ACh-binding protein reveals the ligand-binding domain of nicotinic receptors. Nature 2001;411:269–276.
15. Celie PH, van Rossum-Fikkert SE, van Dijk WJ, Brejc K, Smit AB, Sixma TK. Nicotine and carbamylcholine binding to nicotinic acetylcholine receptors as studied in AChBP crystal structures. Neuron 2004;41:907–914.
16. Bourne Y, Talley TT, Hansen SB, Taylor P, Marchot P. Crystal structure of a Cbtx-AChBP complex reveals essential interactions between snake alpha-neurotoxins and nicotinic receptors. EMBO J 2005;24:1512–1522.
17. Celie PH, Kasheverov IE, Mordvintsev DY, Hogg RC, van Nierop P, van Elk R, van Rossum-Fikkert SE, Zhmak MN, Bertrand D, Tsetlin V, Sixma TK, Smit AB. Crystal structure of nicotinic acetylcholine receptor homolog AChBP in complex with an alpha-conotoxin PnIA variant. Nat Struct Mol Biol 2005;12:582–588.
18. Celie PH, Klaassen RV, van Rossum-Fikkert SE, van Elk R, van Nierop P, Smit AB, Sixma TK. Crystal structure of acetylcholine-binding protein from *Bulinus truncatus* reveals the conserved structural scaffold and sites of variation in nicotinic acetylcholine receptors. J Biol Chem 2005;280:26457–26466.
19. Hansen SB, Sulzenbacher G, Huxford T, Marchot P, Taylor P, Bourne Y. Structures of Aplysia AChBP complexes with nicotinic agonists and antagonists reveal distinctive binding interfaces and conformations. EMBO J 2005;24:3635–3646.
20. Ulens C, Hogg RC, Celie PH, Bertrand D, Tsetlin V, Smit AB, Sixma TK. Structural determinants of selective alpha-conotoxin binding to a nicotinic acetylcholine receptor homolog AChBP. Proc Natl Acad Sci USA 2006;103:3615–3620.
21. Dutertre S, Ulens C, Buttner R, Fish A, van Elk R, Kendel Y, Hopping G, Alewood PF, Schroeder C, Nicke A, Smit AB, Sixma TK, Lewis RJ. AChBP-targeted alpha-conotoxin correlates distinct binding orientations with nAChR subtype selectivity. EMBO J 2007;26:3858–3867.
22. Dellisanti CD, Yao Y, Stroud JC, Wang ZZ, Chen L. Crystal structure of the extracellular domain of nAChR alpha1 bound to alpha-bungarotoxin at 1.94 A resolution. Nat Neurosci 2007;10:953–962.
23. Hilf RJ, Dutzler R. X-ray structure of a prokaryotic pentameric ligand-gated ion channel. Nature 2008;452:375–379.
24. Bocquet N, Nury H, Baaden M, Le Poupon C, Changeux JP, Delarue M, Corringer PJ. X-ray structure of a pentameric ligand-gated ion channel in an apparently open conformation. Nature 2009;457:111–114.
25. Hilf RJ, Dutzler R. Structure of a potentially open state of a proton-activated pentameric ligand-gated ion channel. Nature 2009;457:115–118.
26. Sine SM. The nicotinic receptor ligand binding domain. J Neurobiol 2002;53:431–446.
27. Sine SM, Engel AG. Recent advances in Cys-loop receptor structure and function. Nature 2006;440:448–455.
28. Love RA, Stroud RM. The crystal structure of alpha-bungarotoxin at 2.5 A resolution: relation to solution structure and binding to acetylcholine receptor. Protein Eng 1986;1:37–46.
29. Nomoto H, Takahashi N, Nagaki Y, Endo S, Arata Y, Hayashi K. Carbohydrate structures of acetylcholine receptor from *Torpedo californica* and distribution of oligosaccharides among the subunits. Eur J Biochem 1986;157:233–242.
30. Gehle VM, Sumikawa K. Site-directed mutagenesis of the conserved *N*-glycosylation site on the nicotinic acetylcholine receptor subunits. Brain Res Mol Brain Res 1991;11:17–25.
31. Gehle VM, Walcott EC, Nishizaki T, Sumikawa K. *N*-glycosylation at the conserved sites ensures the expression of properly folded functional ACh receptors. Brain Res Mol Brain Res 1997;45:219–229.
32. Psaridi-Linardaki L, Mamalaki A, Remoundos M, Tzartos SJ. Expression of soluble ligand- and antibody-binding extracellular domain of human muscle acetylcholine receptor alpha subunit in yeast Pichia pastoris. Role of glycosylation in alpha-bungarotoxin binding. J Biol Chem 2002;277:26980–26986.
33. Fruchart-Gaillard C, Gilquin B, Antil-Delbeke S, Le Novere N, Tamiya T, Corringer PJ, Changeux JP, Menez A, Servent D. Experimentally based model of a complex between a snake toxin and the alpha 7 nicotinic receptor. Proc Natl Acad Sci USA 2002;99:3216–3221.
34. Mordvintsev DY, Polyak YL, Levtsova OV, Tourleigh YV, Kasheverov IE, Shaitan KV, Utkin YN, Tsetlin VI. A model for short alpha-neurotoxin bound to nicotinic acetylcholine receptor from *Torpedo californica*: comparison with long-chain alpha-neurotoxins and alpha-conotoxins. Comput Biol Chem 2005;29:398–411.
35. Mordvitsev DY, Polyak YL, Kuzmin DA, Levtsova OV, Tourleigh YV, Utkin YN, Shaitan KV, Tsetlin VI. Computer modeling of binding of diverse weak toxins to nicotinic acetylcholine receptors. Comput Biol Chem 2007;31:72–81.
36. Huang X, Zheng F, Stokes C, Papke RL, Zhan CG. Modeling binding modes of alpha7 nicotinic acetylcholine receptor with ligands: the roles of Gln117 and other residues of the receptor in agonist binding. J Med Chem 2008;51:6293–6302.
37. Yi M, Tjong H, Zhou HX. Spontaneous conformational change and toxin binding in alpha7 acetylcholine receptor: insight into channel activation and inhibition. Proc Natl Acad Sci USA 2008;105:8280–8285.
38. Hu ZJ, Bai L, Tizabi Y, Southerland W. Computational modeling study of human nicotinic acetylcholine receptor for developing new drugs in the treatment of alcoholism. Interdiscip Sci 2009;1:254–262.
39. Bairoch A, Boeckmann B, Ferro S, Gasteiger E. Swiss-Prot: juggling between evolution and stability. Brief Bioinform 2004;5:39–55.
40. Thompson JD, Higgins DG, Gibson TJ. Clustal-W—improving the sensitivity of progressive multiple sequence alignment through sequence weighting. Position-specific gap penalties and weight matrix choice. Nucleic Acids Res 1994;22:4673–4680.

41. Eswar N, John B, Mirkovic N, Fiser A, Ilyin VA, Pieper U, Stuart AC, Marti-Renom MA, Madhusudhan MS, Yerkovich B, Sali A. Tools for comparative protein structure modeling and analysis. Nucleic Acids Res 2003;31:3375–3380.
42. Stuctural Analysis and Verification Server. Available at: http://nih-server.mbi.ucla.edu/SAVES/.
43. Humphrey W, Dalke A, Schulten K. VMD: visual molecular dynamics. J Mol Graph 1996;14:33–38.
44. Case DA, Cheatham TE, III, Darden T, Gohlke H, Luo R, Merz KM, Jr, Onufriev A, Simmerling C, Wang B, Woods RJ. The Amber biomolecular simulation programs. J Comput Chem 2005;26: 1668–1688.
45. Gordon JC, Myers JB, Folta T, Shoja V, Heath LS, Onufriev A. H++: a server for estimating pKas and adding missing hydrogens to macromolecules. Nucleic Acids Res 2005;33:W368–W371.
46. Cornell WD, Cieplak P, Bayly CI, Gould IR, Merz KM, Ferguson DM, Spellmeyer DC, Fox T, Caldwell JW, Kollman PA. A 2nd generation force-field for the simulation of proteins, nucleic-acids, and organic-molecules. J Am Chem Soc 1995;117:5179–5197.
47. Hornak V, Abel R, Okur A, Strockbine B, Roitberg A, Simmerling C. Comparison of multiple amber force fields and development of improved protein backbone parameters. Proteins Struct Funct Bioinform 2006;65:712–725.
48. Kirschner KN, Yongye AB, Tschampel SM, Gonzalez-Outeirino J, Daniels CR, Foley BL, Woods RJ. GLYCAM06: a generalizable biomolecular force field. Carbohydr J Comput Chem 2008;29:622–655.
49. Tsui V, Case DA. Theory and applications of the generalized Born solvation model in macromolecular Simulations. Biopolymers 2000;56:275–291.
50. Miyamoto S, Kollman PA. Settle—an analytical version of the shake and rattle algorithm for rigid water models. J Comput Chem 1992;13:952–962.
51. Cheatham TE, Miller JL, Fox T, Darden TA, Kollman PA. Molecular-dynamics simulations on solvated biomolecular systems—the particle mesh Ewald method leads to stable trajectories of DNA, RNA, and proteins. J Am Chem Soc 1995;117:4193–4194.
52. Berendsen HJC, Postma JPM, Vangunsteren WF, Dinola A, Haak JR. Molecular-dynamics with coupling to an external bath. J Chem Phys 1984;81:3684–3690.
53. Jorgensen WL, Chandrasekhar J, Madura JD, Impey RW, Klein ML. Comparison of simple potential functions for simulating liquid water. J Chem Phys 1983;79:926–935.
54. Nirthanan S, Gwee MC. Three-finger alpha-neurotoxins and the nicotinic acetylcholine receptor, forty years on. J Pharmacol Sci 2004;94:1–17.
55. Zouridakis M, Zisimopoulou P, Poulas K, Tzartos SJ. Recent advances in understanding the structure of nicotinic acetylcholine receptors. IUBMB Life 2009;61:407–423.
56. Betzel C, Lange G, Pal GP, Wilson KS, Maelicke A, Saenger W. The refined crystal structure of alpha-cobratoxin from *Naja naja* siamensis at 2.4-A resolution. J Biol Chem 1991;266:21530–21536.